ACS APPLIED MATERIALS & INTERFACES

Research Article

www.acsami.org

Nanoimprinted Comb Structures in a Low Bandgap Polymer: Thermal Processing and Their Application in Hybrid Solar Cells

Sebastian Dunst,[†,‡] Thomas Rath,[*,†] Andrea Radivo,[§] Enrico Sovernigo,[§,∥] Massimo Tormen,[§,∥] Heinz Amenitsch,[⊥] Benedetta Marmiroli,[⊥] Barbara Sartori,[⊥] Angelika Reichmann,[#] Astrid-Caroline Knall,[†] and Gregor Trimmel[*,†]

[†]Institute for Chemistry and Technology of Materials, Graz University of Technology, Stremayrgasse 9, 8010 Graz, Austria

[‡]Polymer Competence Center Leoben GmbH, Roseggerstraße 12, 8700 Leoben, Austria

[§]IOM CNR, Laboratorio TASC Area Science Park—Basovizza, S.S. 14 Km 163.5, 34149 Trieste, Italy

[∥]ThunderNIL srl, via Ugo Foscolo 8, 35131 Padova, Italy

[⊥]Institute of Inorganic Chemistry, Graz University of Technology, Stremayrgasse 9, 8010 Graz, Austria

[#]Institute for Electron Microscopy and Nanoanalysis, Graz University of Technology & Centre for Electron Microscopy Graz, Steyrergasse 17, 8010 Graz, Austria

Supporting Information

ABSTRACT: In this paper, we investigate conjugated polymer layers structured by nanoimprint lithography toward their suitability for the fabrication of nanostructured polymer/metal sulfide hybrid solar cells. Consequently, we first study the thermal stability of the nanoimprinted conjugated polymer layers by means of scanning electron microscopy and grazing incidence small-angle X-ray scattering, which reveals a reasonable thermal stability up to 145 °C and sufficient robustness against the solvent mixture used in the subsequent fabrication process. In the second part, we demonstrate the preparation of nanostructured polymer/copper indium sulfide hybrid solar cells via the infiltration and thermal decomposition of a mixture of copper and indium xanthates. Although this step needs temperatures of more than 160 °C, the nanostructures are retained in the final polymer/copper indium sulfide layers. The nanostructured solar cells show significantly improved power conversion efficiencies compared to similarly prepared flat bilayer devices, which is based on a distinct improvement of the short circuit current in the nanostructured solar cells.

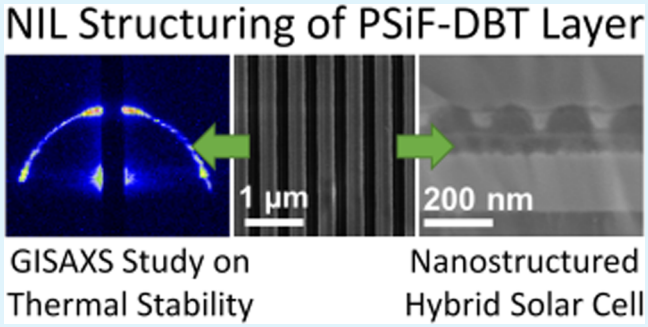

KEYWORDS: *nanoimprint lithography, GISAXS, metal xanthate, copper indium sulfide, organic−inorganic hybrid photovoltaics*

1. INTRODUCTION

Inorganic−organic hybrid solar cells consisting of a mixture of an inorganic nanostructured semiconductor and an organic semiconductor have been researched for more than 15 years. In particular, in the last 5 years, major progress has been achieved by pursuing different strategies[1−3] and power conversion efficiencies have now reached 4−5.5%.[4−6]

The key parameters for obtaining efficient solar cells and the starting points for further improvements are similar to those of polymer−fullerene solar cells: (1) the adjustment of the electronic and optical properties of the donor (usually the organic semiconductor) and the acceptor (inorganic semiconductor), (2) the optimization of the morphology between donor and acceptor and (3) the optimum extraction of the carriers by adjusted electrodes.

Especially the second point, the optimum phase separation and the understanding of its importance to the power conversion efficiencies (PCEs) has tremendously improved the efficiencies of polymer-PCBM ([6,6]-phenyl C_{61} butyric acid methyl ester) solar cells. The optimum phase separation between donor and acceptor is a compromise between a large interface for efficient charge separation (necessary for exciton dissociation in the polymer phase) and continuous (and larger) domains for fast charge transport. There is a plenitude of studies focusing on the issue of how to optimize this nanomorphology (for reviews, see references 7−10).

In the context of organic/inorganic hybrid solar cells, inorganic nanostructures of nonspherical shape (nanorods, tetrapods, clusters) are of interest because these could facilitate charge transport while keeping a large interface.[11] However, a simple mixing of donor and acceptor might lead to isolated nanoparticles in the polymer matrix, which cannot contribute to

Received: February 13, 2014
Accepted: April 14, 2014
Published: April 14, 2014

   dx.doi.org/10.1021/am5009425 | ACS Appl. Mater. Interfaces 2014, 6, 7633−7642

electricity generation as electrons will not find a path to the electrodes. In addition to these issues, the surface of the nanoparticles and in particular the interface between nanoparticle and polymer phase make this field more complicated.[12] Capping ligands are isolating, whereas uncapped nanoparticles may have defects that may act as trap sites.

So far, mainly three methods for the fabrication of hybrid solar cells have been developed.[13] In the classical approach, the nanoparticles are prepared via colloidal synthesis routes, are then subjected to a purification or ligand exchange process in a second step and are finally mixed with a conjugated polymer to form the active layer of the hybrid solar cell. In this approach, a solution of the nanoparticles and polymers is coated onto the electrodes during device fabrication. The ligand-free in situ approach, in which the nanoparticles are directly prepared from precursor materials in the polymer matrix, intends to overcome the problems of ligand exchange and is an interesting alternative route to the classical colloidal approach.[13,14] Following this route, a solution of a nanoparticle-precursor and the conjugated polymer is used for device fabrication. In both methods, the possibilities to control the absorber layer morphology are limited. In the classical approach, different morphologies can be obtained by changing the shape of the nanoparticles (dots, rods, tetrapods); in the in situ route, changing the shape of the nanostructure is more challenging; however, nanorod-type structures also have been already obtained with this method.[15]

The third approach, the "infiltration approach", provides the possibility to obtain highly ordered absorber layers without ligands between the inorganic and organic phase. Here, in a first step, inorganic nanostructured layers are prepared using different techniques like (template assisted) nanorod or nanotube growth,[16,17] UV-lithography,[18] etching,[19,20] or selected area epitaxy processes[21] and are then infiltrated with an organic conjugated polymer to complete the active layer of the solar cell.[22]

Alternatively, the polymeric semiconductor can be nanostructured with techniques like nanoimprint lithography (NIL). The resulting polymer nanostructures are in turn infiltrated with the inorganic component, similar to how it is done for polymer/PCBM solar cells.[8,23−25] This approach, including NIL-structuring, has, regarding possible future large scale production of organic or hybrid solar cells, the advantage that roll-to-roll structuring and processing can be realized.[8] However, in this case, the soft organic material is situated at the bottom of the absorber layer and the hard inorganic material at the top, which is challenging for the processing procedure.

In this study, we explore the preparation of nanostructured polymer/metal sulfide hybrid solar cells by using thermal decomposition of metal xanthates for the formation of the metal sulfide phase on a NIL-structured polymer layer. Metal xanthates have recently been used for the ligand-free fabrication of bulk heterojunction polymer/metal sulfide nanoparticle hybrid solar cells,[26−30] and can be also used for this approach because of their ability to be converted into the metal sulfide without byproducts remaining in the metal sulfide layer already at comparably low temperatures.[26] Regarding the thermal management, it would be more convenient to structure the metal xanthate layer first, but due to the crystallinity and the low thermal stability of the metal xanthates, this is not possible.

2. EXPERIMENTAL SECTION

2.1. Sample Preparation. Poly[9,9-dioctyl-2,7-silafluorene-co-*alt*-5,5-(4′,7′-di-2-thienyl-2′,1′,3′-benzothiadiazole)] (PSiF-DBT) films deposited either on silicon for the GISAXS study or on glass/ITO/PEDOT:PSS for the solar cell study were patterned by thermal nanoimprint lithography (NIL).[31]

For the GISAXS study, the PSiF-DBT films on silicon were imprinted using a PW 20 E press (Paul-Otto Weber GmbH) at 125 °C and 6 MPa in ambient atmosphere. To prevent potential deterioration of the electronic properties of the conjugated polymer by oxidative degradation, for the hybrid solar cells the PSiF-DBT films were imprinted in a glovebox filled with nitrogen at 5 MPa and 150 °C using a homemade thermal NIL press. As NIL stamps, silicon gratings with periodicities of 180 or 500 nm or their copies on glass/Ormostamp (microresist technologies GmbH) were used after functionalization of their surfaces with a monolayer of octadecyl trichlorosilane assembled from vapor phase as an antiadhesion agent. Ormostamp replicas of the silicon masters were prepared by UV-NIL structuring of an Ormostamp resist on glass substrates.[32,33]

To describe the NIL-structuring process briefly, the stamp and sample are put face-to-face onto the plate of the press, the heating ramp is started and after reaching the preset imprinting temperature, pressure is applied and maintained for 5 min. Subsequently, the hot plates are cooled down to 40 °C, the pressure is released and the stamp and sample are manually separated.

The hybrid solar cells were fabricated on glass/ITO substrates (Xinyan Technology Ltd., Hong Kong) with a sheet resistance of 10 Ω/sq, which were cleaned in deionized water and isopropyl alcohol in an ultrasonic bath followed by O_2 plasma cleaning (FEMTO, Diener Electronic, Germany). The PEDOT:PSS layer (Clevios P VP.Al 4083, Heraeus) was spin coated on the glass/ITO layer and subsequently annealed at 150 °C for 10 min in a glovebox. As a second layer, PSiF-DBT (1-Material, Chemsitech Inc., Canada) was coated by doctor blading on the PEDOT:PSS layer from a chloroform solution (10 mg/mL), which was partly nanostructured by NIL (as described above) in a further step.

The precursor layer for the copper indium sulfide (CIS) layer, consisting of a copper and indium xanthate mixture (12.1 mg/mL, 1 equiv copper *O*-2,2-dimethylpentan-3-yl dithiocarbonate; 54.6 mg/mL, 1.6 equiv (for annealing at 160 °C) or 55.4 mg/mL, 1.7 equiv (for annealing at 195 °C) indium *O*-2,2-dimethylpentan-3-yl dithiocarbonate; metal xanthates were obtained from Aglycon, Austria) dissolved in the solvent mixture isopropyl alcohol:dichloromethane:-pyridine = 4:2:1 (vol:vol:vol) was deposited by doctor blading. The coating step was followed by a thermal conversion step at a temperature of 160 or 195 °C on a programmable heating plate (CAT Ingenieurbüro M. Zipperer GmbH, Germany; temperature program: heating with a rate of 11 °C/min to a temperature of 160 or 195 °C and a holding time at this temperature for 30 min (160 °C) and 15 min (195 °C), respectively). The synthesis of the xanthate precursors and the thermal conversion step in order to obtain CIS nanoparticles has been described previously.[26] The about 200 nm thick aluminum electrodes were deposited via thermal evaporation.

2.2. Characterization. Scanning electron microscopy (SEM) images of the NIL-structured polymer layers were acquired on a Zeiss Supra 40 scanning electron microscope, analyses of cross sections of the prepared solar cells were conducted on a Zeiss Ultra 55 electron microscope; the cross sections for these characterizations were realized by large area ion milling using a Gatan Ilion+. Layer thicknesses were determined on a Bruker DekTak XT surface profiler.

Two-dimensional (2D) grazing incidence small-angle X-ray scattering (GISAXS) measurements were performed at the Austrian SAXS Beamline 5.2L of the electron storage ring ELETTRA (Italy),[34] using a similar setup as described before.[35] The beamline has been adjusted to a q-resolution ($q = 4\pi/\lambda^*\sin(2\theta/2)$, 2θ represents the scattering angle) between 0.1 and 3.1 nm^{-1} (GISAXS). The X-ray energy was 8 keV. The nanostructured samples were placed in a modified heating cell (DHS 1100 from Anton Paar GmbH, Graz, Austria) with a custom-made dome with a grazing angle of about 0.18°

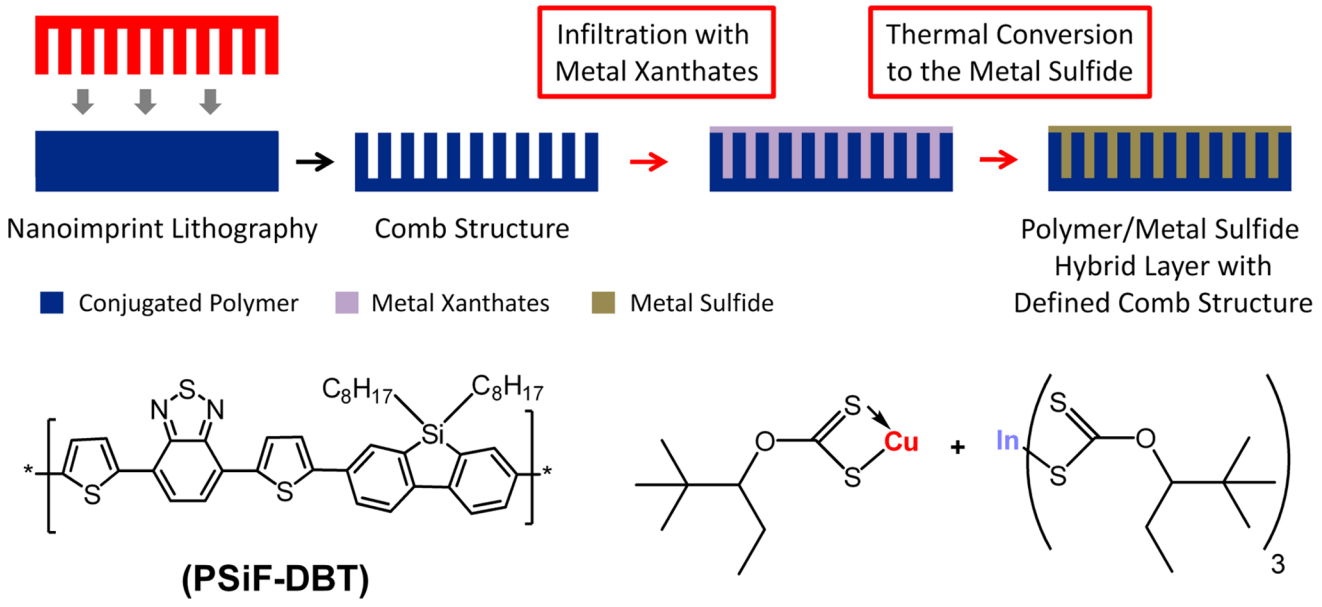

Figure 1. Schematic illustration of the NIL process for the preparation of comb structures and the infiltration process toward defined hybrid layers and chemical structures of the used polymer PSiF-DBT and the Cu and In xanthates.

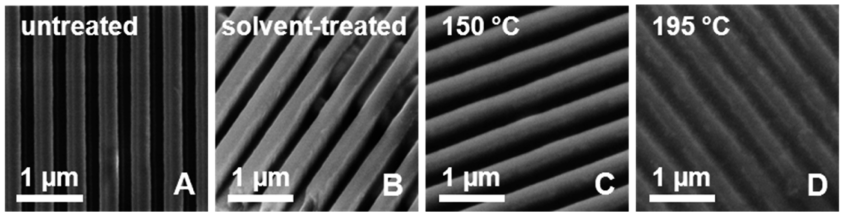

Figure 2. SEM images of NIL-imprinted comb structures (periodicity 500 nm); (A) after the NIL step, (B) after NIL and solvent treatment and (C, D) after NIL and subsequent temperature treatment at 150 or 195 °C.

and were heated from 35 °C up to 200 °C at a heating rate of approximately 10 °C min^{-1} under nitrogen atmosphere. The NIL-imprinted line structures were aligned parallel to the X-ray beam. During the temperature scan, data were recorded with 11 s time resolution using an image intensified CCD detector (GemStar/XIDIS model, Photonic Science Ltd., Millham/U.K.). For detection of the grazing incidence wide-angle X-ray scattering (GIWAXS) signal, a two-dimensional hybrid pixel array detector system (Pilatus 100 K, Dectris) was used. The angular calibration of the detectors was carried out using silver behenate powder (*d*-spacing of 58.38 Å).

PCE values of the solar cells were determined from IV curves recorded using a Keithley 2400 SourceMeter, a custom-made LabView software and a Dedolight DLH400D lamp. The light intensity was set to 100 mW/cm^2, providing a spectrum quite similar to AM1.5G (determined using a KippZonen-CMP-11 pyranometer, no spectral mismatch was considered).

3. RESULTS AND DISCUSSION

Figure 1 schematically depicts the process steps for the fabrication of nanostructured polymer/metal sulfide absorber layers for hybrid solar cells using NIL for structuring of the polymer and metal xanthates as precursors for the metal sulfide. First, a comb structure is imprinted in the conjugated polymer PSiF-DBT. Second, the structured layer is coated with a metal xanthate solution and finally, the metal xanthates are thermally converted to a metal sulfide layer. During this preparation process, besides the NIL-structuring, the stability of the nanostructures against solvents used for coating the metal xanthates as well as the thermal stability of the nanostructures during the thermal conversion of the metal xanthates to the sulfides are critical issues, which are investigated in this work.

For the NIL-structuring of the low bandgap polymer PSiF-DBT (poly[9,9-dioctyl-2,7-silafluorene-co-*alt*-5,5-(4′,7′-di-2-thienyl-2′,1′,3′-benzothiadiazole)]$_n$, the chemical structure is given in Figure 1), we started with the optimized standard parameters for thermal nanoimprint lithography (NIL) used for structuring of poly(3-hexylthiophene) (P3HT), i.e., 100 °C and 6 MPa.

From these starting values, we found that for PSiF-DBT, the temperature had to be increased to or above 125 °C to accurately reproduce gratings of 500 and 180 nm periodicity. The actual samples used in the GISAXS study were made in ambient atmosphere and consisted of PSiF-DBT films on silicon imprinted at 13 MPa and 125 °C. The samples used for the fabrication and the study of photovoltaic cells were made on ITO coated glass substrates, and the PSiF-DBT film was imprinted at 5 MPa and 150 °C in a glovebox with nitrogen atmosphere, owing to reduced concerns about polymer degradation and better imprinting results.

For optimizing the processing parameters and preliminary thermal stability studies, defined comb structures with a periodicity of 500 nm were imprinted in the PSiF-DBT layer. A SEM image of such a layer is shown in Figure 2A. The height of the structures is approximately 260−270 nm (see Figure S1 in the Supporting Information). For further studies and fabrication of solar cells, comb structures with a periodicity of 180 nm were prepared.

dx.doi.org/10.1021/am5009425 | *ACS Appl. Mater. Interfaces* 2014, 6, 7633−7642

After the NIL-structuring process, for the realization of nanostructured hybrid solar cells via the "xanthate route", it was important to find a suitable solvent for applying the metal xanthate layer on the nanostructured polymer layer, which provides sufficient wettability, but does not harm or even erase the imprinted nanostructures. Therefore, in a first step, experiments were conducted to find proper solvents for this process step by immersing nonstructured flat polymer layers on glass substrates in a series of different solvents and solvent combinations, which have the capability of readily dissolving the copper as well as the indium xanthate. Among the tested solvents (chloroform, dichloromethane, toluene, chlorobenzene, DMF, aceton, THF, isopropyl alcohol) a mixture of isopropyl alcohol, dichloromethane and pyridine (4:2:1 vol:vol:vol) turned out to be the most promising one, as it did not dissolve the polymer layer at all even after immersion for more than 24 h. Additionally, we also evaluated the stability of a nanostructured layer against this solvent combination by immersing the layer for 1 min, which is about the time for which the nanostructured sample is actually in contact with the solvent during the doctor blading step in the course of solar cell fabrication. The SEM image in Figure 2B proves that the nanostructured layer withstands the solvent treatment and the defined rectangular shape of the comb structure is retained. The partial filling of the nanostructures (visible in the upper right part of the image) can be assigned to undefined drying of the layer after solvent treatment and will not have an influence on the nanostructured polymer/CIS heterojunction.

A further crucial issue to realize hybrid solar cells following this route is a sufficient thermal stability of the nanostructures in the conjugated polymer layer, as the metal xanthates have to be thermally converted to yield the metal sulfide. Thus, we characterized the influence of thermal treatment of the structured polymer layers by means of SEM and time-resolved GISAXS. Comparing the SEM micrographs of a pristine NIL-structured polymer layer (Figure 2A) with those of layers after heat treatment for 15 min at 150 °C (Figure 2C) and 195 °C (Figure 2D), it is clearly visible that the untreated sample has line structures with comparably sharp edges, which appear softer in the sample annealed at 150 °C and which became quite blurred in the sample heated to 195 °C. This rough analysis suggests that the line structures are still present after a temperature treatment of 150 °C, which is sufficient for the formation process of the copper indium sulfide layer without destroying the polymer nanostructures. However, also a remainder of the structural motif is still clearly visible after heating to 195 °C.

For the time-resolved GISAXS study on the thermal stability of the imprinted line structures, a nanostructured layer was heated in a measuring cell (under nitrogen atmosphere) directly in the X-ray beam. For these measurements, nanostructured layers with a periodicity of 180 nm were used, as it was intended to apply layers with this periodicity in hybrid solar cells. Thus, these results are not directly comparable with the SEM measurements presented in Figure 2. The GISAXS patterns of a nanostructured PSiF-DBT film on a silicon substrate at different temperatures (65, 105, 143 and 200 °C) during the heating run to 200 °C (heating rate: 10 °C/min) are shown in Figure 3. At temperatures lower than 120 °C, a semicircle-like chain of intensity maxima is visible, which is typical for periodic line structures oriented parallel to the X-ray beam.[36,37] The maximum in the out-of-plane position is given by the intersection of the truncation rods inclined with the

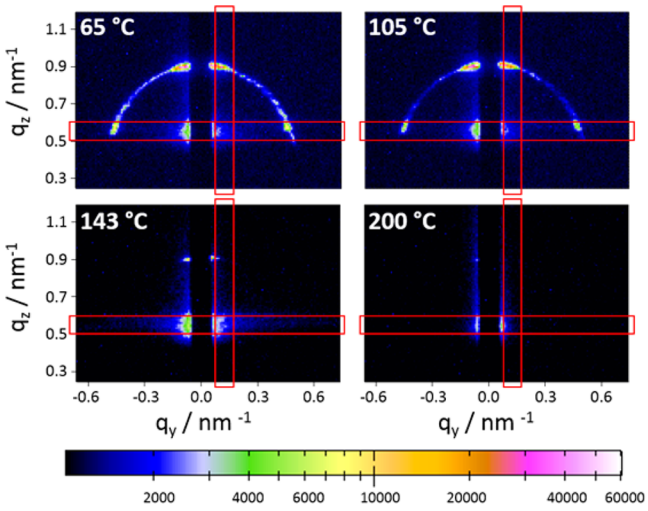

Figure 3. GISAXS images of a NIL-structured PSiF-DBT film (periodicity: 180 nm) at 65, 105, 143 and 200 °C. The red boxes indicate the vertical and horizontal areas for integration.

grazing angle and the Ewald sphere. The inclination angle was 0.63° in this case. Similar patterns have been observed for NIL-structured polymer layers.[38] Further, the thermal stability has also been investigated for 4 μm NIL structures by the group of Müller-Buschbaum.[39] By further increasing the temperature, this semicircle-like pattern vanishes and only a feature near to the beam stop, which represents also the most intense area of the semicircle at lower temperatures, remains.

In Figure 4A, the evolution of the out-of-plane scattering (retrieved by integration of vertical cuts of the GISAXS patterns) with increasing temperature is shown. At low temperatures, the scattering signal exhibits two distinct peaks, the contribution of the in-plane wings of the Yoneda peak integrated in the out-of-plane direction at around q_z = 0.55 nm^{-1} and the peak stemming from the periodic line structure caused by the truncation rod scattering at approximately q_z = 0.9 nm^{-1}. The latter is visible up to a temperature of 143 °C, before it vanishes. The in-plane cuts showing a similar behavior are presented in Figure 4B. The effect of the NIL structure decomposition is visualized in more detail in Figure 4C, where the temperature-dependent intensity of this peak (obtained from fitting of the peak with Lorentzian function) is plotted. The intensity stays almost constant up to a temperature of about 110 °C. At this temperature, the peak starts to become weaker until it decreases steeply at 130 °C. From these changes, it can be assumed that the glass transition temperature of PSiF-DBT is about 110 °C or even below, although it could not be experimentally determined by differential scanning calorimetry (DSC) measurements by us and others.[40] Above a temperature of 140−145 °C, the peak is not detectable any more in the out-of-plane scattering signal. The intensity of the wings of the Yoneda peak with increasing temperature is shown in Figure 4D. The intensity increases in the same temperature range in which the "line structure peak" steeply decreases. The increase in the out-of-plane intensity of the wings of the Yoneda peak indicates that the nanostructured polymer layer becomes rougher in this temperature range, which leads to the conclusion that the ordered well-defined layer has changed to a rougher and more disordered structure. At a later stage of the heating run, at about 180 °C, the out-of-plane intensity decreases again, which is an artifact, as observed in the in-plane-

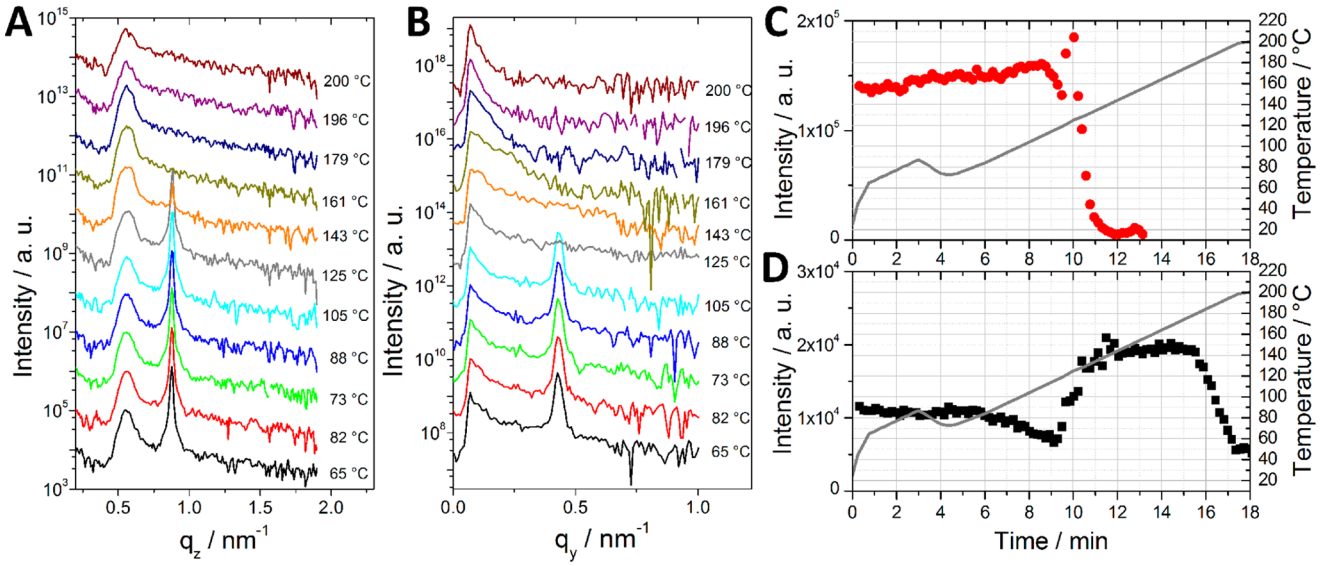

Figure 4. Evolution of the out-of-plane (A) and in-plane (B) scattering signal of a NIL-structured PSiF-DBT film (periodicity: 180 nm) during a heating run to 200 °C with a heating rate of 10 °C/min, approximately every 10th measurement is shown, the curves are shifted vertically for better visibility; (C) temperature-dependent changes in out-of-plane intensity of the "line structure peak" at approximately q_z = 0.9 nm^{-1}; (D) temperature-dependent changes in out-of-plane intensity of the wings of the Yoneda peak at approximately q_z = 0.55 nm^{-1}.

cuts of Figure 4B. Here the roughness increases again due to the changes of the slope, which might be an indication for a further blurring of the material.

As already stated before, the results on the thermal stability obtained from GISAXS measurements cannot be directly compared with these obtained from SEM images. The SEM images were mainly acquired to get a first indication about the thermal behavior of the samples and were done with samples having periodic line structures of 500 nm, which were annealed on a simple laboratory heating plate without cover, while the GISAXS measurements were done inside a calibrated heating cell using samples with a periodic line structure of 180 nm. Both the small uncertainty concerning temperature of the laboratory heating plate and the different periodicities of the line structures can explain the slightly higher temperature stability of the nanostructures observed by SEM.

However, according to the results of the SEM as well as the GISAXS analyses, the two criteria for a possible realization of a nanostructured polymer/CIS hybrid layer, a reasonable thermal and solvent stability, are fulfilled.

In a further step, the formation of a CIS layer on the nanostructured polymer film from copper and indium xanthates was investigated by a combined time-resolved GIWAXS/GISAXS experiment. Therefore, a nanostructured polymer layer on a silicon substrate was coated with a copper and indium xanthate layer via doctor blading and after drying, the sample was subsequently heated to 200 °C (heating rate 10 °C/min) in the same measuring cell.

The GISAXS images of the sample at different temperatures during one heating run are presented in Figure 5 and the areas for vertical integration are indicated with red boxes. The resulting out-of-plane scattering signals at q_y = 0.058 nm^{-1} of the GISAXS patterns are shown in Figure 6A. Because the nanoimprinted comb structure is now covered by a dense layer of the metal xanthates and later in the heating run with a metal sulfide layer, no signal of the comb structure is detected in this case. The pronounced change in the GISAXS pattern at a temperature between 155 and 173 °C stems from increased

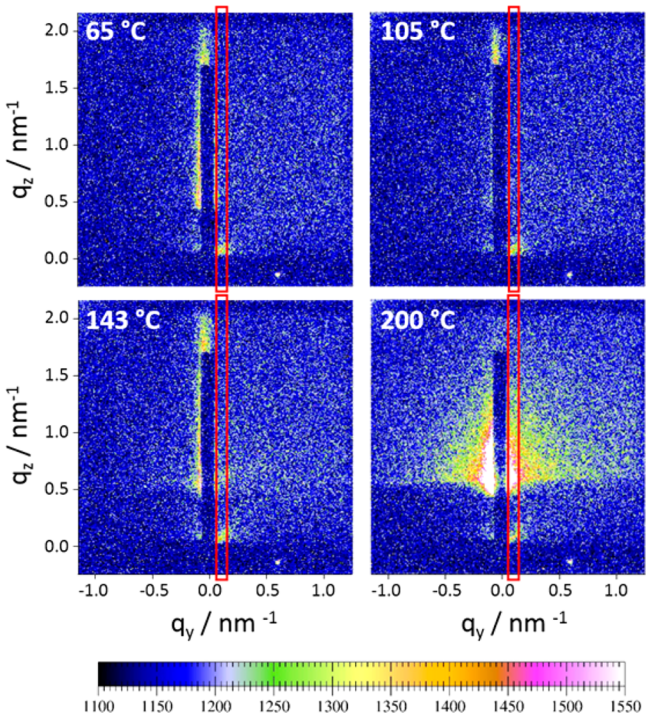

Figure 5. GISAXS images of the nanostructured polymer film (periodicity: 180 nm) covered with metal xanthates at different temperatures during the heating run from room temperature to 200 °C. The red boxes indicate the vertical areas for integration.

diffuse scattering of the sample. This can be explained by the fact that the metal xanthates decompose during the heating run, organic decomposition products evaporate out of the layer and a film consisting of CIS nanocrystals is formed. Due to the evaporation of decomposition products and the increased density of the CIS nanoparticles compared to the metal xanthates, the volume of the film shrinks, going along with an increase of porosity, which is visible in the GISAXS patterns. The patterns at higher temperatures follow a power law

dx.doi.org/10.1021/am5009425 | ACS Appl. Mater. Interfaces 2014, 6, 7633−7642

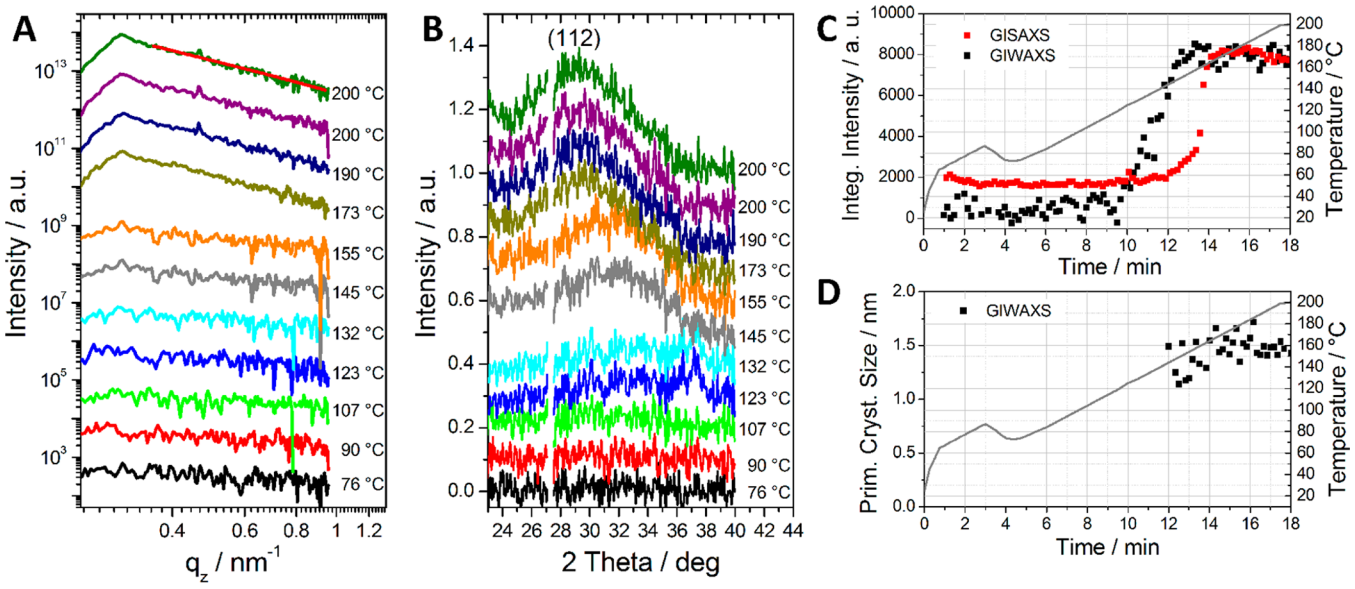

Figure 6. Temperature-dependent evolution of the vertical cuts of the GISAXS patterns of the nanostructured polymer film (periodicity: 180 nm) covered with metal xanthates (A) and the (112) peak of CIS in the GIWAXS signal (B) during a heating run to 200 °C with a heating rate of 10 °C/min. Approximately every 10th measurement is shown. For better visibility, the vertical cuts as well as the X-ray patterns are shifted vertically; (C) Porod invariant "Q" of the GISAXS as well as integrated intensity of the GIWAXS patterns calculated between 0.58 and 1.70 nm^{-1} as well as 24 and 38° 2θ, respectively, plotted versus reaction time and temperature; (D) primary crystallite size in the nanocrystalline CIS layer estimated using Scherrer equation.

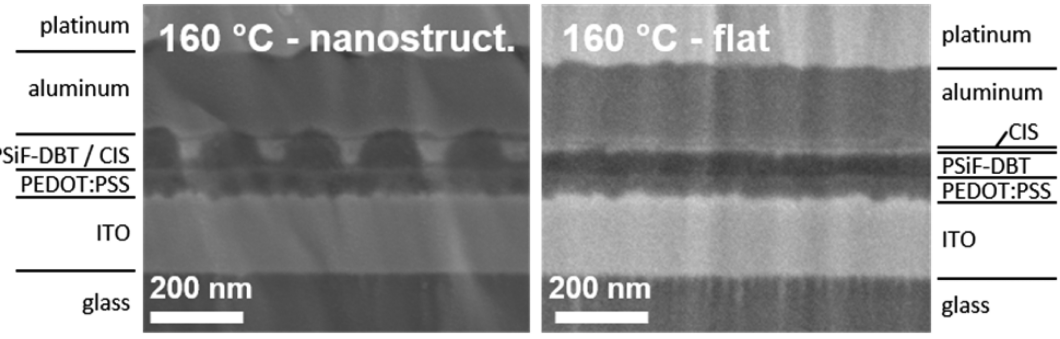

Figure 7. SEM images of cross sections of hybrid solar cells comprising a polymer/CIS absorber layer with nanostructured (periodicity: 180 nm) as well as flat interface prepared at 160 °C.

behavior ($I(q) \propto (q_y^2 + q_z^2)^{-\alpha/2}$) with a Porod exponent of 2.72. This value is typical for porous structures with a large size distribution. One power law fit is exemplarily shown as a red line in Figure 6A for the GISAXS pattern measured at 200 °C. No indications of particle scattering have been observed in the measured q-regime. The small peak at q_z = 0.46 nm^{-1} is due to the broadening of the specular reflected beam caused in the in-plane direction by the increased surface roughness of the copper and indium xanthate layer after decomposition and heating, therefore, it becomes visible in the out-of-plane cuts.

The GIWAXS signals acquired during the heating run are depicted in Figure 6B. It is clearly visible that the (112) peak of CIS is detectable in the 2θ range of 29−30° starting at a temperature of about 140 °C. This issue is outlined in more detail in Figure 6C, where the evolution of the integrated intensity of the GIWAXS pattern calculated between 24 and 38° 2θ is plotted versus reaction time and temperature. Additionally, the Porod invariant "Q"[41] (see the Supporting Information), which represents the volume fraction of the structures, has been plotted for comparison. The intensity of the GIWAXS signal starts to increase at a heating time of about 10 min, which corresponds to a temperature of 125−130 °C. At a temperature of about 150 °C, the increase of the signal ceases. From then on, the signal stays constant until the end of the heating run, which indicates that the formation of the CIS phase seems to be completed at about this temperature. The Porod invariant derived from the GISAXS measurements increases a bit later in the heating run (at approximately 155 °C), when the formation of the CIS nanoparticles has been just completed and also the decomposition products have evaporated from the layer, indicating an increasing porosity of the film in this stage of the heating run.

Figure 6D shows that the primary crystallite size in the nanocrystalline CIS layer, which was estimated using the Scherrer equation and the full width at half-maximum of the (112) peak obtained from fitting of the peak with Lorentzian function, is about 1.5 nm. Therefore, these structures are too small to be resolved by the GISAXS measurements due to the limited q-range. Nevertheless, this finding points out that the conversion of the metal xanthates to the CIS phase is initiated shortly before the nanoimprinted line structure starts to become slightly blurred, which is at about 140−145 °C. This,

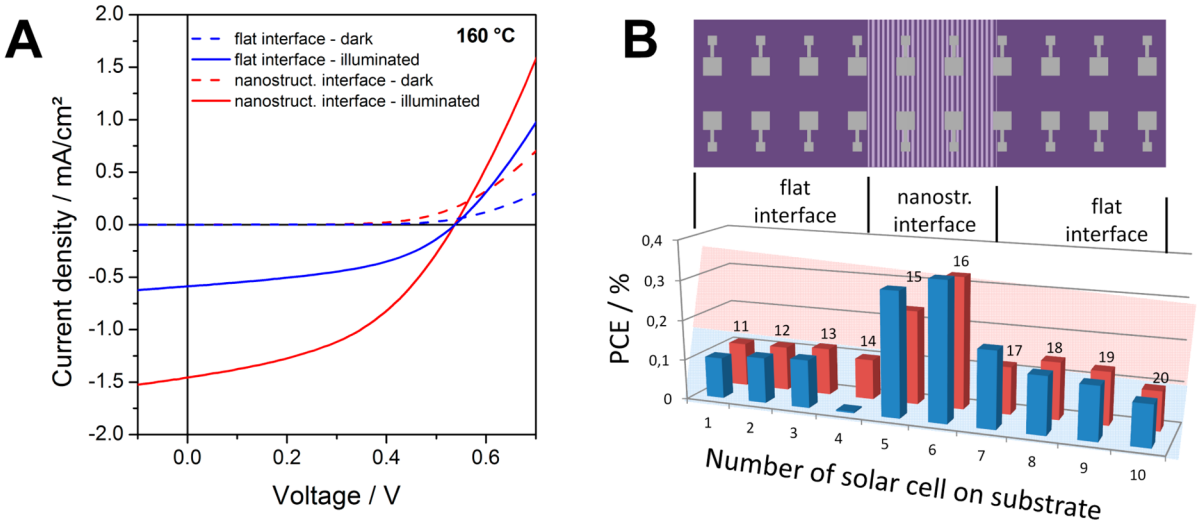

Figure 8. (A) IV curves measured in the dark and under 100 mW/cm^2 illumination of hybrid solar cells with flat and nanostructured (periodicity: 180 nm) interfaces prepared at 160 °C and (B) distribution of PCEs of solar cells with flat and nanostructured interfaces over one typical substrate; position 4 was short circuited.

Table 1. Characteristic Parameters of Hybrid Solar Cells with Flat and Nanostructured (Periodicity: 180 nm) Interfaces Prepared at 160 °C

	temp (°C)	interface	V_{OC} (V)	I_{SC} (mA/cm^2)	FF (%)	PCE (%)
values from IV curves in Figure 8A	160	flat	0.537	0.59	45.5	0.14
		nanostructured	0.537	1.46	44.6	0.34
mean values and std deviations	160	flat	0.532 ± 0.009	0.58 ± 0.02	43.7 ± 2.0	0.13 ± 0.1
		nanostructured	0.537 ± 0.007	1.32 ± 0.18	43.4 ± 1.1	0.30 ± 0.04

in turn, leads to the conclusion that a realization of a nanostructured polymer/CIS absorber layer should be possible, as we also assume that once the CIS layer is formed on the polymeric nanostructure, it should provide a certain support to the polymer line structure, even at higher temperatures.

Thus, the next step was to prepare hybrid solar cells with a NIL-structured polymer/CIS hybrid absorber layer. For this purpose, nanoimprinted line structures in PSiF-DBT were prepared on glass/ITO/PEDOT:PSS/PSiF-DBT samples. The total sample area was 7.5 × 2.4 cm, whereby only about 2.4 × 2.4 cm in the middle of the substrate were nanostructured. Thus, the influence of the nanostructuring compared to a flat polymer/CIS bilayer geometry on the solar cell performance could be directly determined and compared on a single substrate, on which the structured and nonstructured parts were further processed in exactly the same way. After NIL-structuring, a mixed copper and indium xanthate solution (solvent mixture: isopropyl alcohol, dichloromethane, pyridine (4:2:1 vol:vol:vol)) was applied to the partly nanostructured PSiF-DBT layer by doctor blading, whereby no differences in wetting were observed during the coating process between structured and nonstructured areas. Subsequently, the substrates were heated to 160 °C to form the CIS layer on the polymer and the solar cell fabrication was finally finished with the deposition of aluminum electrodes via thermal evaporation.

The SEM images of ion polished cross sections of as prepared hybrid solar cells with nanostructured and flat interfaces, respectively, are presented in Figure 7. The about 150 nm thick ITO layer is covered by an approximately 30 nm thick PEDOT:PSS layer. In the cross section of the nanostructured solar cell, it is evident that the approximately 100 nm thick nanostructured polymer layer is filled with CIS. In the flat bilayer absorber layer, the 50 nm thick polymer layer is covered by a CIS layer with a thickness of about 20 nm. The aluminum electrode has a thickness of approximately 170 nm.

Figure 8A shows the IV curves of the hybrid solar cells with the flat and nanostructured hybrid interface prepared at an annealing temperature of 160 °C. The characteristic parameters extracted from the IV curves are summarized in Table 1. Figure 8B shows the power conversion efficiencies of all 20 solar cells prepared on one substrate. The positions 5, 6, 15 and 16 had a nanostructured absorber layer, whereas the other solar cells had a flat interface between PSiF-DBT and CIS. It can be clearly seen that the average PCE of the solar cells with flat interface lies between 0.1 and 0.15%, whereas the devices with nanostructured interface exhibit values around 0.3%. This improvement in PCE is attributable to an increased I_{SC} in the nanostructured device (I_{SC} – flat interface, 0.5–0.6 mA/cm^2; I_{SC} – nanostructured interface, 1.4–1.5 mA/cm^2). The V_{OC} as well as the FF stay constant at values of 537 mV and 45%, respectively. The mean values and their standard deviations of the characteristic parameters of typical solar cells with flat and nanostructured interface prepared at 160 °C are also given in Table 1. Furthermore, it is interesting to note that the slope of both the dark and the illuminated IV curves of the nanostructured device is significantly steeper, which suggests a decreased series resistance (R_S) in the nanostructured devices (R_S – flat interface, ∼235 Ω·cm^2; R_S – nanostructured interface, ∼125 Ω·cm^2).

Furthermore, we investigated polymer/CIS hybrid solar cells prepared at 195 °C instead of 160 °C, a temperature at which the imprinted nanostructure in the PSiF-DBT layer is definitely not well-defined (see Figure 2D). The SEM image of a cross section of such a solar cell prepared at 195 °C (Figure 9A)

dx.doi.org/10.1021/am5009425 | ACS Appl. Mater. Interfaces 2014, 6, 7633–7642

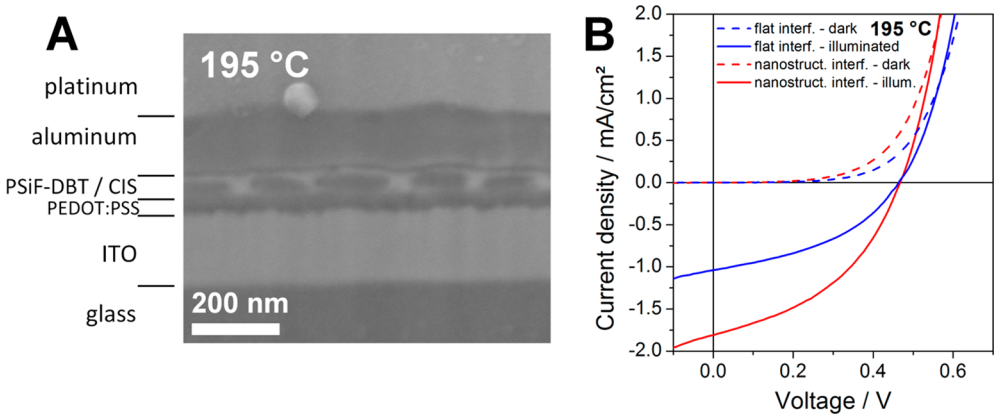

Figure 9. (A) SEM image of an ion polished cross section of a hybrid solar cell with nanostructured interface prepared at 195 °C, (B) IV curves measured in the dark and under 100 mW/cm^2 illumination of hybrid solar cells with flat and nanostructured interface prepared at 195 °C. The solar cells were prepared using nanostructured polymer films with a periodicity of 180 nm.

Table 2. Characteristic Parameters of Hybrid Solar Cells with Flat and Nanostructured Interfaces Prepared at 195 °C[a]

	temp (°C)	interface	V_{OC} (V)	I_{SC} (mA/cm^2)	FF (%)	PCE (%)
values from IV curves in Figure 9B	195	flat	0.467	1.04	41.3	0.20
		nanostructured	0.467	1.81	42.3	0.35
mean values and std deviations	195	flat	0.474 ± 0.008	1.10 ± 0.08	41.7 ± 0.4	0.22 ± 0.01
		nanostructured	0.459 ± 0.008	1.74 ± 0.08	41.9 ± 0.6	0.33 ± 0.01

[a]The solar cells were prepared using nanostructured polymer films with a periodicity of 180 nm.

exhibits, as expected, that the nanostructure has changed significantly. It seems that the comb structures deliquesce, though remains of the periodic structures are still visible. The IV curves of the prepared solar cells, shown in Figure 9B, exhibit a similar picture to the one described for the devices prepared at 160 °C. Also in this case, the R_S of the solar cell with the nanostructured interface is lower (R_S – flat interface, ~150 Ω·cm^2; R_S – nanostructured interface, ~80 Ω·cm^2) and the I_{SC} of the device with nanostructured interface is about 80% higher than that of the device with flat interface. The V_{OC} as well as FF are similar, which results in a significant difference in PCE – flat interface, 0.2%; nanostructured interface, 0.35% (see Table 2).

4. CONCLUSION

On the basis of this study, it can be concluded that the preparation of nanostructured polymer/metal sulfide hybrid solar cells using NIL for structuring a conjugated polymer layer, which is coated with a metal xanthate solution and subsequently thermally annealed at moderate temperatures to form the inorganic metal sulfide on the nanostructure, is generally feasible. The performed temperature resolved GISAXS study revealed that a very good thermal stability of the polymer nanostructures is given up to a temperature of 130–140 °C. Above this temperature, the nanostructure is slightly blurred, as was seen in the SEM images. SEM images also indicated that the polymer nanostructures are sufficiently thermally stable, so that at an annealing temperature of 160 °C, the imprinted line structure is largely maintained in the polymer phase. At an annealing temperature of 195 °C, the nanostructure appears much more blurred in the SEM images. Moreover, the stability of the nanostructures against the solvent used for dissolving the metal xanthates, a mixture of isopropyl alcohol, dichloromethane and pyridine turned out not to be a critical issue in the solar cell fabrication process.

The nanostructured solar cells prepared at 160 and 195 °C show a significantly improved power conversion efficiency compared to similarly prepared flat bilayer devices, which is based on a distinct improvement of the short circuit current in the nanostructured solar cells. To further optimize nanostructured hybrid solar cells prepared via this approach, the temperature of the annealing step has to be kept as low as possible in order to retain a very defined nanostructure. A reduction of the annealing temperature could be achieved by addition of amines to the metal xanthate solution, which were recently shown to facilitate crystallization of the metal sulfide at lower temperatures.[42] Therefore, we assume that by optimizing the imprinting process and imprinting nanostructures with smaller periodicities as well as applying lower annealing temperatures to form the metal sulfide phase, the power conversion efficiencies of such nanostructured hybrid solar cells should be significantly improved.

■ ASSOCIATED CONTENT

Supporting Information

Additional SEM image and analytical expression for the Porod invariant "Q". This material is available free of charge via the Internet at http://pubs.acs.org.

■ AUTHOR INFORMATION

Corresponding Authors

*T.R. Tel: +43 316 873 32281. Fax: +43 316 873 1032281. E-mail: thomas.rath123@gmail.com.

*G.T. Tel: +43 316 873 32281. Fax: +43 316 873 1032281. E-mail: gregor.trimmel@tugraz.at.

Author Contributions

The paper was written through contributions of all authors. All authors have given approval to the final version of the paper.

Funding

Part of the research work was performed in the project IV-1.02 of the Polymer Competence Center Leoben GmbH (PCCL, Austria) within the framework of the COMET-program of the Austrian Ministry for Transport, Innovation and Technology and the Austrian Ministry of Economy, Family and Youth with contributions by academic and commercial partners. The PCCL is funded by the Austrian Government and the State Governments of Styria and Upper Austria.

Notes

The authors declare no competing financial interest.

■ ACKNOWLEDGMENTS

GISAXS and GIWAXS measurements were carried out at the Austrian SAXS beamline at Elettra Trieste. The authors thank Sebastian Rauch and Sanja Simic for their help with the SEM measurements.

■ REFERENCES

(1) Gao, F.; Ren, S.; Wang, J. The Renaissance of Hybrid Solar Cells: Progresses, Challenges, and Perspectives. *Energy Environ. Sci.* **2013**, *6*, 2020−2040.

(2) Zhou, R.; Xue, J. Hybrid Polymer−Nanocrystal Materials for Photovoltaic Applications. *ChemPhysChem* **2012**, *13*, 2471−2480.

(3) Wright, M.; Uddin, A. Organic - Inorganic Hybrid Solar Cells: A Comparative Review. *Sol. Energy Mater. Sol. Cells* **2012**, *107*, 87−111.

(4) Chen, Z.; Zhang, H.; Du, X.; Cheng, X.; Chen, X.; Jiang, Y.; Yang, B. From Planar-Heterojunction to n−i Structure: An Efficient Strategy to Improve Short-Circuit Current and Power Conversion Efficiency of Aqueous-Solution-Processed Hybrid Solar Cells. *Energy Environ. Sci.* **2013**, *6*, 1597−1603.

(5) Zhou, R.; Stalder, R.; Xie, D.; Cao, W.; Zheng, Y.; Yang, Y.; Plaisant, M.; Holloway, P. H.; Schanze, K. S.; Reynolds, J. R.; Xue, J. Enhancing the Efficiency of Solution-Processed Polymer:Colloidal Nanocrystal Hybrid Photovoltaic Cells Using Ethanedithiol Treatment. *ACS Nano* **2013**, *7*, 4846−4854.

(6) Liu, Z.; Sun, Y.; Yuan, J.; Wei, H.; Huang, X.; Han, L.; Wang, W.; Wang, H.; Ma, W. High-Efficiency Hybrid Solar Cells Based on Polymer/PbS_xSe_{1-x} Nanocrystals Benefiting from Vertical Phase Segregation. *Adv. Mater.* **2013**, *25*, 5772−5778.

(7) Liu, F.; Yu, G.; Jung, J. W.; Jo, W. H.; Russell, T. P. On the Morphology of Polymer-Based Photovoltaics. *J. Polym. Sci., Part B: Polym. Phys.* **2012**, *50*, 1018−1044.

(8) Yang, Y.; Mielczarek, K.; Aryal, M.; Zakhidov, A.; Hu, W. Nanoimprinted Polymer Solar Cell. *ACS Nano* **2012**, *6*, 2877−2892.

(9) Wang, M.; Wudl, F. Top-Down Meets Bottom-Up: Organized Donor−Acceptor Heterojunctions for Organic Solar Cells. *J. Mater. Chem.* **2012**, *22*, 24297−24314.

(10) Chen, J.-T.; Hsu, C.-S. Conjugated Polymer Nanostructures for Organic Solar Cell Applications. *Polym. Chem.* **2011**, *2*, 2707−2722.

(11) Gur, I.; Fromer, N. A.; Chen, C.-P.; Kanaras, A. G.; Alivisatos, A. P. Hybrid Solar Cells with Prescribed Nanoscale Morphologies Based on Hyperbranched Semiconductor Nanocrystals. *Nano Lett.* **2007**, *7*, 409−414.

(12) Chen, H.-C.; Lai, C.-W.; Wu, I.-C.; Pan, H.-R.; Chen, I.-W. P.; Peng, Y.-K.; Liu, C.-L.; Chen, C.-H.; Chou, P.-T. Enhanced Performance and Air Stability of 3.2% Hybrid Solar Cells: How the Functional Polymer and CdTe Nanostructure Boost the Solar Cell Efficiency. *Adv. Mater.* **2011**, *23*, 5451−5455.

(13) Rath, T.; Trimmel, G. In Situ Syntheses of Semiconducting Nanoparticles in Conjugated Polymer Matrices and Their Application in Photovoltaics. *Hybrid Mater.* **2013**, *1*, 15−36.

(14) Martinez-Ferrero, E.; Albero, J.; Palomares, E. Materials, Nanomorphology, and Interfacial Charge Transfer Reactions in Quantum Dot/Polymer Solar Cell Devices. *J. Phys. Chem. Lett.* **2010**, *1*, 3039−3045.

(15) Kaltenhauser, V.; Rath, T.; Haas, W.; Torvisco, A.; Müller, S. K.; Friedel, B.; Kunert, B.; Saf, R.; Hofer, F.; Trimmel, G. Bismuth Sulphide−Polymer Nanocomposites From a Highly Soluble Bismuth Xanthate Precursor. *J. Mater. Chem. C* **2013**, *1*, 7825−7832.

(16) Conradt, J.; Sartor, J.; Thiele, C.; Maier-Flaig, F.; Fallert, J.; Kalt, H.; Schneider, R.; Fotouhi, M.; Pfundstein, P.; Zibat, V.; Gerthsen, D. Catalyst-Free Growth of Zinc Oxide Nanorod Arrays on Sputtered Aluminum-Doped Zinc Oxide for Photovoltaic Applications. *J. Phys. Chem. C* **2011**, *115*, 3539−3543.

(17) Bao, N.; Feng, X.; Grimes, C. A. Self-Organized One-Dimensional TiO_2 Nanotube/Nanowire Array Films for Use in Excitonic Solar Cells: A Review. *J. Nanotechnol.* **2012**, 645931.

(18) Rath, T.; Padeste, C.; Vockenhuber, M.; Fradler, C.; Edler, M.; Reichmann, A.; Letofsky-Papst, I.; Hofer, F.; Ekinci, Y.; Griesser, T. Direct Extreme UV-Lithographic Conversion of Metal Xanthates Into Nanostructured Metal Sulfide Layers for Hybrid Photovoltaics. *J. Mater. Chem. A* **2013**, *1*, 11135−11140.

(19) Pudasaini, P. R.; Ruiz-Zepeda, F.; Sharma, M.; Elam, D.; Ponce, A.; Ayon, A. A. High Efficiency Hybrid Silicon Nanopillar−Polymer Solar Cells. *ACS Appl. Mater. Interfaces* **2013**, *5*, 9620−9627.

(20) Jeong, S.; Garnett, E. C.; Wang, S.; Yu, Z.; Fan, S.; Brongersma, M. L.; McGeehe, M. D.; Cui, Y. Hybrid Silicon Nanocone−Polymer Solar Cells. *Nano Lett.* **2012**, *12*, 2971−2976.

(21) Mariani, G.; Wang, Y.; Wong, P.-S.; Lech, A.; Hung, C.-H.; Shapiro, J.; Prikhodko, S.; El-Kady, M.; Kaner, R. B.; Huffaker, D. L. Three-Dimensional Core−Shell Hybrid Solar Cells via Controlled in Situ Materials Engineering. *Nano Lett.* **2012**, *12*, 3581−3586.

(22) Weickert, J.; Dunbar, R. B.; Hesse, H. C.; Wiedemann, W.; Schmidt-Mende, L. Nanostructured Organic and Hybrid Solar Cells. *Adv. Mater.* **2011**, *23*, 1810−1828.

(23) He, X.; Gao, F.; Tu, G.; Hasko, D. G.; Hüttner, S.; Greenham, N. C.; Steiner, U.; Friend, R. H.; Huck, W. T. S. Formation of Well-Ordered Heterojunctions in Polymer:PCBM Photovoltaic Devices. *Adv. Funct. Mater.* **2011**, *21*, 139−146.

(24) Moungthai, S.; Mahadevapuram, N.; Ruchhoeft, P.; Stein, G. E. Direct Patterning of Conductive Polymer Domains for Photovoltaic Devices. *ACS Appl. Mater. Interfaces* **2012**, *4*, 4015−4023.

(25) Chen, D.; Zhao, W.; Russell, T. P. P3HT Nanopillars for Organic Photovoltaic Devices Nanoimprinted by AAO Templates. *ACS Nano* **2012**, *6*, 1479−1485.

(26) Rath, T.; Edler, M.; Haas, W.; Fischereder, A.; Moscher, S.; Schenk, A.; Trattnig, R.; Sezen, M.; Mauthner, G.; Pein, A.; Meischler, D.; Bartl, K.; Saf, R.; Bansal, N.; Haque, S. A.; Hofer, F.; List, E. J. W.; Trimmel, G. A Direct Route Towards Polymer/Copper Indium Sulfide Nanocomposite Solar Cells. *Adv. Energy Mater.* **2011**, *1*, 1046−1050.

(27) Arar, M.; Gruber, M.; Edler, M.; Haas, W.; Hofer, F.; Bansal, N.; Reynolds, L. X.; Haque, S. A.; Zojer, K.; Trimmel, G.; Rath, T. Influence of Morphology and Polymer:Nanoparticle Ratio on Device Performance of Hybrid Solar Cells − An Approach in Experiment and Simulation. *Nanotechnology* **2013**, *24*, 484005.

(28) Rath, T.; Kaltenhauser, V.; Haas, W.; Reichmann, A.; Hofer, F.; Trimmel, G. Solution-Processed Small Molecule/Copper Indium Sulfide Hybrid Solar Cells. *Sol. Energy Mater. Sol. Cells* **2013**, *114*, 38−42.

(29) Leventis, H. C.; King, S. P.; Sudlow, A.; Hill, M. S.; Molloy, K. C.; Haque, S. A. Nanostructured Hybrid Polymer−Inorganic Solar Cell Active Layers Formed by Controllable in Situ Growth of Semiconducting Sulfide Networks. *Nano Lett.* **2010**, *10*, 1253−1258.

(30) Bansal, N.; O'Mahony, F. T. F.; Lutz, T.; Haque, S. A. Solution Processed Polymer−Inorganic Semiconductor Solar Cells Employing Sb_2S_3 as a Light Harvesting and Electron Transporting Material. *Adv. Energy Mater.* **2013**, *3*, 986−990.

(31) Chou, S. Y.; Krauss, P. R.; Renstrom, P. J. Nanoimprint Lithography. *J. Vac. Sci. Technol., B: Microelectron. Nanometer Struct.–Process., Meas., Phenom.* **1996**, *14*, 4129−4133.

(32) Schift, H.; Spreu, C.; Saidani, M.; Bednarzik, M.; Gobrecht, J.; Klukowska, A.; Reuther, F.; Grützner, G.; Solak, H. H. Transparent Hybrid Polymer Stamp Copies with Sub-50-nm Resolution for

Thermal and UV-Nanoimprint Lithography. *J. Vac. Sci. Technol., B: Microelectron. Nanometer Struct.–Process., Meas., Phenom.* **2009**, *27*, 2846−2849.
(33) Mühlberger, M.; Bergmair, I.; Klukowska, A.; Kolander, A.; Leichtfried, H.; Platzgummer, E.; Loeschner, H.; Ebm, C.; Grützner, G.; Schöftner, R. UV-NIL with Working Stamps Made from Ormostamp. *Microelectron. Eng.* **2009**, *86*, 691−693.
(34) Amenitsch, H.; Rappolt, M.; Kriechbaum, M.; Mio, H.; Laggner, P.; Bernstorff, S. First Performance Assessment of the Small-Angle X-Ray Scattering Beamline at ELETTRA. *J. Synchrotron Radiat.* **1998**, *5*, 506−508.
(35) Fischereder, A.; Rath, T.; Haas, W.; Amenitsch, H.; Schenk, D.; Zankel, A.; Saf, R.; Hofer, F.; Trimmel, G. Investigation of $CuInS_2$ Thin Film Formation by a Low-Temperature Chemical Deposition Method. *ACS Appl. Mater. Interfaces* **2012**, *4*, 382−390.
(36) Wernecke, J.; Scholze, F.; Krumrey, M. Direct Structural Characterisation of Line Gratings with Grazing Incidence Small-Angle X-Ray Scattering. *Rev. Sci. Instrum.* **2012**, *83*, 103906.
(37) Yan, M.; Gibaud, A. On the Intersection of Grating Truncation Rods With the Ewald Sphere Studied by Grazing-Incidence Small-Angle X-Ray Scattering. *J. Appl. Crystallogr.* **2007**, *40*, 1050−1055.
(38) Rueda, D. R.; Martín-Fabiani, I.; Soccio, M.; Alayo, N.; Pérez-Murano, F.; Rebollar, E.; García-Gutiérrez, M. C.; Castillejo, M.; Ezquerra, T. A. Grazing-Incidence Small-Angle X-Ray Scattering of Soft and Hard Nanofabricated Gratings. *J. Appl. Crystallogr.* **2012**, *45*, 1038−1045.
(39) Meier, R.; Chiang, H.-Y.; Ruderer, M. A.; Guo, S.; Körstgens, V.; Perlich, J.; Müller-Buschbaum, P. In Situ Film Characterization of Thermally Treated Microstructured Conducting Polymer Films. *J. Polym. Sci., Part B: Polym. Phys.* **2012**, *50*, 631−641.
(40) Boudreault, P.-L. T.; Michaud, A.; Leclerc, M. A New Poly(2,7-Dibenzosilole) Derivative in Polymer Solar Cells. *Macromol. Rapid Commun.* **2007**, *28*, 2176−2179.
(41) Porod, G. In *Small-Angle X-ray Scattering*; Glatter, O., Kratky, O., Eds.; Academic Press: London, 1982; pp 46−48.
(42) Bansal, N.; Reynolds, L. X.; MacLachlan, A.; Lutz, T.; Ashraf, R. S.; Zhang, W.; Nielsen, C. B.; McCulloch, I.; Rebois, D. G.; Kirchartz, T.; Hill, M. S.; Molloy, K. C.; Nelson, J.; Haque, S. A. Influence of Crystallinity and Energetics on Charge Separation in Polymer-Inorganic Nanocomposite Films for Solar Cells. *Sci. Rep.* **2013**, *3*, 1531.